Journal of the Chinese Society of Mechanical Engineers, Vol.47, No.4, pp341~352 (2026)

# Numerical Study of a Laminar Confined Slot-Impinging Jet with a Baffle

Feng Yang Wu*, Wen-Ren Jong**and Yu-Chin Chien***

**Keywords:** jet impingement, baffle, computational fluid dynamics, flow structure, heat transfer

## Abstract

In this paper, a two-dimensional simulation of a laminar confined slot-impinging jet with a baffle is conducted. A constant temperature is imposed on the bottom wall, while the other walls are treated as adiabatic. ANSYS Fluent, a commercial computational fluid dynamics (CFD) software is used to solve the governing equations. The mesh setting is validated by comparing numerical predictions of pressure coefficient and stagnation point Nusselt number with previous studies in the literature. The effects of baffle distance ( $5 \le d/W \le 25$ ), height ( $0.5 \le h_b/W \le 1.5$ ), and width ( $0.5 \le w_b/W \le 8.0$ ) on fluid flow and heat transfer at different Reynolds numbers ( $100 \le \mathrm{Re} \le 400$ ) were numerically analyzed. Two mechanisms (guided flow and secondary impingement) are identified, depending on the baffle location. Vortices consistently form around the baffle, enhancing mixing and heat transfer. As Reynolds number increases, the average Nusselt number increases while the friction factor decreases. Closer baffle placements can reduce flow resistance at high Reynolds numbers, while distant baffles generally raise resistance but improve heat transfer. Optimal thermal performance occurs at a baffle distance of $d/W = 10$, height $h_b/W = 1.0$, and width $w_b/W = 8$ at $\mathrm{Re} = 400$, achieving a maximum performance evaluation criterion ( PEC ) of 1.0225. The results suggest that appropriate baffle geometry can effectively balance enhanced heat transfer and flow resistance, offering design guidance for thermal optimization in confined slot jet systems.

*Paper Received February, 2025. Revised June, 2025, Accepted June, 2025, Author for Correspondence: Yu-Chin Chien.*

* *Ph.D. Candidate, Department of Mechanical Engineering, Chung Yuan Christian University, Taoyuan 32023, Taiwan, ROC.*

** *Professor, Department of Mechanical Engineering, Chung Yuan Christian University, Taoyuan 32023, Taiwan, ROC.*

*** *Assistant Professor, Department of Mechanical Engineering, Chung Yuan Christian University, Taoyuan 32023, Taiwan, ROC.*

## Nomenclature

| | |
|---|---|
| $c_p$ | constant-pressure specific heat, $\mathrm{J/kg \cdot K}$ |
| $\mathrm{C_p}$ | pressure coefficient, $\mathrm{C_p} = p - p_{in} / (1/2)\rho v_{in}^2$ |
| $d$ | baffle distance, m |
| f | friction factor, $\mathrm{f} = 2W\Delta p / L\rho v_{in}^2$ |
| $h_b$ | baffle height, m |
| $H$ | channel height, m |
| $L$ | channel length, m |
| Nu | Nusselt number, $\mathrm{Nu} = \dot{q}_w W / \lambda (T_w - T_{in})$ |
| $p$ | pressure, Pa |
| PEC | performance evaluation criterion, $\mathrm{PEC} = (\mathrm{Nu/Nu_o}) / (\mathrm{f/f_o})^{1/3}$ |
| $\dot{q}_w$ | impingement surface heat flux, $\mathrm{W/m^2}$ |
| Re | Reynolds number, $\mathrm{Re} = \rho v_{in} W / \mu$ |
| $T$ | temperature, K |
| $u$ | velocity component in the $x$ direction, m/s |
| $v$ | velocity component in the $y$ direction, m/s |
| $w_b$ | baffle width, m |
| $W$ | slot width, m |
| Greek symbols | |
| $\lambda$ | thermal conductivity, $\mathrm{W/m \cdot K}$ |
| $\mu$ | viscosity, $\mathrm{kg/m \cdot s}$ |
| $\rho$ | density, $\mathrm{kg/m^3}$ |
| Subscript | |
| $in$ | inlet condition |
| s | stagnation point |
| $n$ | normal direction |
| o | original state |
| $w$ | wall |

# INTRODUCTION

Jet impingement cooling has gained significant attention as an efficient method for localized heat transfer, particularly within constrained environments where heat dissipation needs to be maximized. Applications of impinging jets span from electronic component cooling to gas turbine blade cooling and high-precision manufacturing, where controlled heat transfer is critical (Hussain et al. (2021), Oliveira et al. (2025)). The use of confined slot jets, specifically, offers advantages in managing the boundary layers and achieving uniform temperature distribution across the target surface (Molana and Banooni (2013)). The fundamental heat transfer processes in liquid jet impingement systems can be identified in three main flow regions: the free jet zone, the impingement zone, and the wall jet zone. These zones are associated with distinctive thermal and fluid dynamic characteristics, particularly in confined systems where interactions between the wall and the jet become more pronounced (Chou and Hung 1994). Several studies reveal that channel configurations can significantly alter flow characteristics. Lee et al. (2008) showed that by varying jet-to-target distances, tighter spacing significantly amplified heat transfer in the impingement zone by increasing boundary layer compression. Yousefi-Lafouraki et al. (2014) studied laminar forced convection within converging channels, demonstrating that reduced outlet widths amplified the impinging jet's thermal impact due to the concentrated jet flow path. This design effectively accelerated flow towards the target surface, enhancing thermal dissipation near the stagnation zone. Similarly, Pulat and Beyazoglu (2021) investigated the effect of wall inclination, demonstrating that inclined channels increase turbulence, allowing for more efficient heat transfer due to accelerated flow and modified pressure gradients.

With the rise of advanced thermal management needs, nanofluids have gained prominence for their superior thermal conductivity compared to conventional fluids. Several studies examined the behavior of nanofluids in confined slot-impinging jets, finding that their high thermal conductivity significantly increased heat transfer rates, especially near the stagnation point (Manca et al. (2011), Lorenzo et al. (2012), Manca et al. (2016)). Mookherjee et al. (2020) investigated confined laminar jet impingement cooling systems using nanofluids, which produced considerable improvements in cooling efficiency under various Reynolds numbers. The enhanced performance was attributed to the improved thermal properties of nanofluids and the formation of a more effective thermal boundary layer at the impingement site. Besides, multiple impinging jets, rather than single jet configurations, have also been investigated to extend the cooling effect over larger areas Selimefendigil et al. (2021). Seyedein et al. (1995) investigated the turbulent flow and heat transfer characteristics of multiple confined impinging slot jets, finding that while multi-jet setups provided more uniform temperature distribution, crossflow interactions led to diminished cooling efficiency in downstream jets. An experimental study by Yalçinkaya et al. (2024) investigated the influence of nozzle lengths on the heat transfer performance of smooth and conical pinned target surfaces. The results indicated that the combination of multi-jet impingement and conical pins significantly improved heat transfer on the target surface. Weng et al. (2025) experimentally examined the heat transfer behavior of single and doublet liquid jets impinging on a heated plate, demonstrating that the atomization induced by the double jets enhances the heat transfer in the hydraulic jump region. Xu et al. (2021) examined screw-thread nozzle jets impinging on concave surfaces and reported that under the same flow conditions, multi-jet arrays provided superior cooling performance compared to single jets due to the cumulative cooling effect.

Swirling flows, which impart a rotational component to the fluid, increase flow complexity and enhance heat transfer rates, have also been employed to improve heat transfer in jet impingement systems. Herrada et al. (2009) investigated confined swirling jets impinging on flat plates, finding that moderate swirl intensities effectively increased local Nusselt numbers while maintaining steady flow conditions. Singh et al. (2023) further extended the analysis to inclined swirling jets, demonstrating that the jet-to-target spacing and swirl intensity significantly impacted the thermal performance. For instance, at reduced jet-to-target distances, swirling jets exhibited higher heat transfer rates than traditional cylindrical jets due to improved impingement intensity. In addition to spiral nozzles, the internal structure of the channel can also improve the mixing of the flow. The insertion of obstacles, such as fins or baffles, within jet impingement setups is another strategy that has demonstrated substantial heat transfer improvements. Qiu et al. (2017) analyzed the effects of conjugate air jet impingement on finned heat sinks, showing that strategically positioned fins effectively increased surface area exposure to the impinging jet, resulting in a 25% increase in overall heat transfer. Maghrabie et al. (2023) focused on guiding baffles in confined air jet setups, observing that baffles close to the stagnation zone promoted flow turbulence and maintained high heat transfer coefficients even under varying flow conditions. Gupta et al. (2024) studied the effectiveness of the confined jet impingement cooling technique for highly concentrated photovoltaic thermal systems. A temperature uniformity of 6.3ºC was achieved using a modified mini-channel heat sink geometry with a single jet inlet at a mass flow rate of 50 g/min. By directing airflow along a desired path and preventing laminarization, these obstacles played a crucial role in stabilizing the Nusselt number distribution across the surface. The use of baffles is not limited to enhancing flow reattachment alone; it also facilitates increased turbulence in strategic zones, which boosts convective heat transfer without the need for higher fluid velocities or Reynolds numbers, making it an energy-efficient solution. For example, several studies on backward-facing steps have also investigated the impact of baffles on convective heat transfer. Nie et al. (2009) investigated separated convection flow over backward-facing steps, showing that strategically placed baffles could double the heat transfer rate by altering reattachment length and promoting turbulence in the recirculation zones. Mohammed et al. (2015) examined the combined effect of baffles and nanofluids, finding nearly a 40% improvement in heat transfer due to the increased thermal conductivity and flow reorganization facilitated by the baffle. Kumar and Vengadesan (2018) demonstrated that baffles placed near reattachment points in laminar flows could enhance Nusselt numbers by 50%, confirming that baffles play a critical role in confined jet systems by directing fluid flow and enhancing heat transfer efficiency.

Building upon the foundational understanding derived from various studies that have meticulously investigated the dynamics of confined and baffled jet impingement systems, it is posited that the thoughtful integration of baffles within the intricate configurations of slot jet systems presents a substantial opportunity for significantly enhancing thermal performance, especially within the context of controlled, laminar flow conditions that are characterized by their orderly and predictable behavior. The motivation behind this study stems from the need to address specific challenges in confined slot jet impingement systems, particularly regarding the improvement of cooling performance through design modifications. Building on prior research, this study numerically investigates the synergistic effects of the baffle distance, height, and width, along with flow velocity, in a laminar confined slot-impinging jet environment.

## MATHEMATICAL MODEL

### Physical Model Description

The schematic diagram of the convective heat transfer of a two-dimensional confined slot-impinging jet with a baffle is illustrated in Figure 1. The computational domain consists of a confined channel with a heated surface at the bottom, and a slot jet inlet that introduces a laminar flow of fluid directed toward the heated surface. The slot width $W$, channel height $H$ and channel length $L$ are considered 6.2 mm, 12.4 mm, and 620 mm, respectively. A baffle with height $h_b$ and width $w_b$ is mounted on the upper wall at a distance $d$ from the center of jet entrance. A constant temperature of $T_w$ ( $313\ \mathrm{K}$ ) is applied to the bottom wall, while the other walls are considered to be adiabatic surfaces with no-slip boundary conditions. The working fluid is considered to be a Newtonian and incompressible fluid flow. The thermophysical properties of water for $293\ \mathrm{K}$ are given in Table 1.

Table 1 Thermophysical properties for working fluid.

| Property | Water |
|---|---|
| $\rho$ ( $\mathrm{kg/m^3}$ ) | 998.2 |
| $c_p$ ( $\mathrm{J/kg \cdot K}$ ) | 4182 |
| $\mu$ ( $\mathrm{kg/m \cdot s}$ ) | 0.000993 |
| $\lambda$ ( $\mathrm{W/m \cdot K}$ ) | 0.597 |

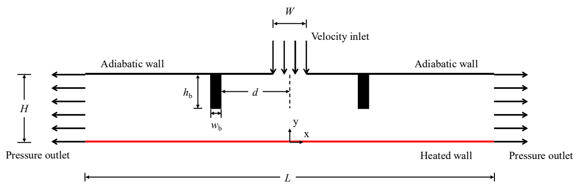


Fig. 1. Schematic diagram of a 2D confined slot-impinging jet with a baffle and coordinate system.

### Governing Equations

Consider the slot-impinging jet flow in a horizontal confined channel is laminar and steady state flow. The two-dimensional governing equations of continuity, momentum, and energy in the Cartesian coordinates are given as

Continuity equation

$$\frac{\partial u}{\partial x}+\frac{\partial v}{\partial y}=0\,. \tag{1}$$

Momentum equations

$$\frac{\partial}{\partial x}(\rho uu)+\frac{\partial}{\partial y}(\rho uv)=-\frac{\partial p}{\partial x}+\mu\left(\frac{\partial^2 u}{\partial x^2}+\frac{\partial^2 u}{\partial y^2}\right), \tag{2}$$

$$\frac{\partial}{\partial x}(\rho uv)+\frac{\partial}{\partial y}(\rho vv)=-\frac{\partial p}{\partial x}+\mu\left(\frac{\partial^2 v}{\partial x^2}+\frac{\partial^2 v}{\partial y^2}\right). \tag{3}$$

Energy equation

$$\frac{\partial}{\partial x}\left(\rho c_p uT\right)+\frac{\partial}{\partial y}\left(\rho c_p vT\right)=\lambda\left(\frac{\partial^2 T}{\partial x^2}+\frac{\partial^2 T}{\partial y^2}\right). \tag{4}$$

### Boundary Conditions

The boundary conditions are set as follows:

At the channel inlet section:

$$u=0\,,\quad v=-v_{in}\,,\ \text{and}\quad T=293\ \mathrm{K}\,. \tag{5}$$

At the channel outlet section:

$$\frac{\partial u}{\partial x}=0\,,\quad \frac{\partial v}{\partial x}=0\,,\ \text{and}\quad \frac{\partial T}{\partial x}=0\,. \tag{6}$$

On the upper and baffle walls:

$$u=v=0\quad \text{and}\quad \frac{\partial T}{\partial n}=0\,, \tag{7}$$

10.29979/JCSME.202608_47(4).0004

where the $n$ represents the normal direction.
On the bottom wall:

$$T_w = 313\,\mathrm{K}. \tag{8}$$

**Analysis Parameters**

In order to analyze the flow and thermal fields and their corresponding characteristics in the confined slot-impinging jet with a baffle, the relevant equations are shown below.

The Reynolds number ( $\mathrm{Re}$ ):

$$\mathrm{Re} = \frac{\rho v_{in} W}{\mu}. \tag{9}$$

The pressure coefficient ( $\mathrm{C_p}$ ):

$$\mathrm{C_p} = \frac{p - p_{in}}{(1/2)\rho v_{in}^2}. \tag{10}$$

The friction factor ( $\mathrm{f}$ ):

$$\mathrm{f} = \frac{2W\Delta p}{L\rho v_{in}^2}, \tag{11}$$

where $\Delta p$ is the pressure difference between the inlet and outlet.

The Nusselt number of the bottom wall ( $\mathrm{Nu}$ ):

$$\mathrm{Nu} = \frac{\dot{q}_w W}{\lambda (T_w - T_{in})}, \tag{12}$$

where $\dot{q}_w$ is the impingement surface heat flux.

The performance evaluation criterion ( $\mathrm{PEC}$ ):

$$\mathrm{PEC} = \frac{(\mathrm{Nu}/\mathrm{Nu_o})}{(\mathrm{f}/\mathrm{f_o})^{1/3}}, \tag{13}$$

where $\mathrm{Nu_o}$ and $\mathrm{f_o}$ represent the Nusselt number and the friction factor in the original confined slot-impinging jet, respectively.

**Numerical Procedure**

In order to reduce the calculation time, the width of the computation domain is reduced to half of the actual width of the confined slot-impinging jet channel, and a symmetry boundary condition is further exploited on the centerline ( $x = 0$ ). The governing equations (1)-(4) were discretized with the aid of the finite volume method using the commercial software ANSYS-Fluent, according to the associated initial and boundary conditions. The coupled algorithm with least squares cell-based gradient is used to solve the pressure-velocity coupling fields. The second-order scheme is adopted in the pressure interpolation and the second-order upwind scheme is utilized in the momentum and energy equations. The convergence criterion for the absolute residuals in the velocity components and energy are assumed to be $10^{-5}$ and $10^{-8}$, respectively.

## GRID DISTRIBUTION AND VALIDATION STUDY

The computational domain is discretized using a structured grid. The mesh is refined near the entrance to capture detailed variations in the boundary layer and thermal gradients, as shown in Figure 2. A grid independence study was conducted to ensure that the simulation results are independent of the grid resolution. Four different grid settings are tested on the model with a $H/W$ ratio of 4 at a Reynolds number of 400, using water as the working fluid, and the details of these grid settings are presented in Table 2. As reported in Figure 3, the results obtained from the third and fourth mesh configurations show very close agreement in terms of stagnation point and average Nusselt number, with negligible relative errors. In order to save calculation time, the grid setting of number 3 is chosen for the subsequent simulation.

The numerical results for the pressure coefficient and the stagnation point Nusselt number obtained using different grid settings are compared with the previously published data by Lee et al. (2008) and Chou and Hung (1994) for the case with a $H/W$ ratio of 4 and Reynolds numbers, ranging from 50 to 400. Both Figure 4 and Figure 5 show a good agreement between the present results and the previous studies.

Table 2 Detailed information on the grid settings.

| Grid no. | Grid nodes |
|---|---|
| 1 | 40,400 |
| 2 | 161,600 |
| 3 | 646,400 |
| 4 | 2,585,600 |

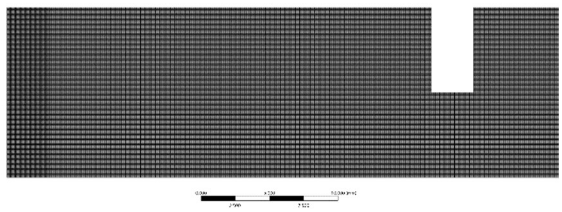

Fig. 2. Mesh configuration for computational domain.

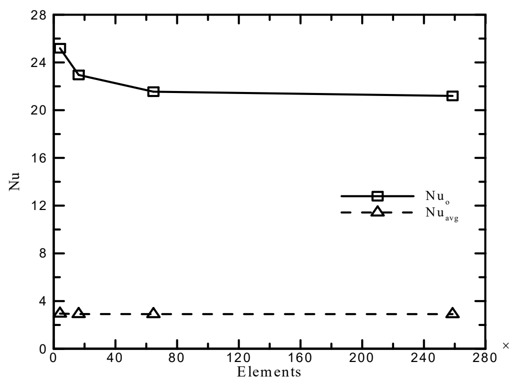


Fig. 3. Grid independent test results on average and stagnation point Nusselt number.

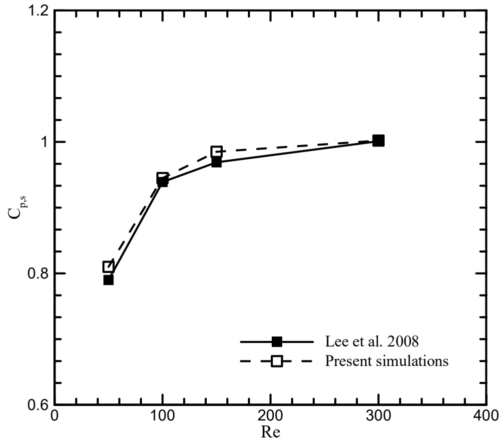


Fig. 4. Validation of pressure coefficient ( $H/W = 4$ ).

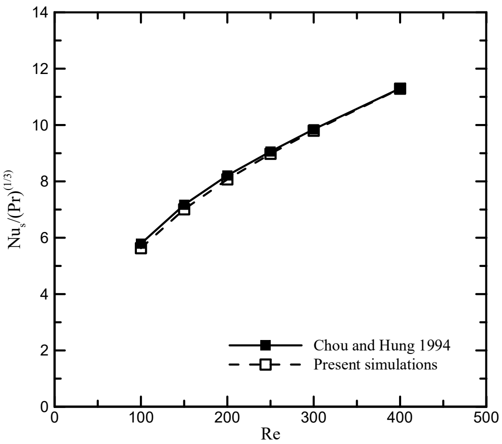


Fig. 5. Validation of stagnation point Nusselt number ( $H/W = 4$ ).

## RESULTS AND DISCUSSION

The flow and heat transfer characteristics of the confined slot-impinging water jet with a baffle are numerically investigated in this section. The effects of Reynolds number and baffle distance on the local Nusselt number, average Nusselt number, and pressure coefficient are first discussed. Subsequently, the influences of baffle height and width are further examined. Parametric analysis is performed over the ranges of $100 \le Re \le 400$ , $5 \le d/W \le 25$ , $0.5 \le h_b/W \le 1.5$, and $0.5 \le w_b/W \le 8.0$.

The effects of Reynolds number and baffle distance on the local Nusselt number distribution are shown in Figures 6–10. Figure 6 illustrates the local Nusselt number along the heated wall at Reynolds numbers in the range of 100−400 for the normal case. The local Nusselt number drops sharply from the initial peak, reaches a valley, then gradually rises to a second peak, and finally approaches to a steady value. In general, the valley and peak of the local Nusselt number decrease and increase, respectively, as the Reynolds number increases, and both of the valley and the second peak gradually shift downstream along the channel. Subsequently, the following discussion considers the case where the baffle height ratio $h_b/W$ is maintained at 1.0, while the width ratio $w_b/W$ is maintained at 0.5. Figures 7–10 describe the local Nusselt number along the heated wall at Reynolds numbers in the range of 100−400, corresponding to $d/W$ values of 5, 10, 15, and 25, respectively. It can be seen that the local Nusselt number has a double valley and a more acute peak due to the action of the baffle. This means that the presence of the baffle can further enhance the local heat transfer phenomenon. As the Reynolds number increases, the local Nusselt number varies more dramatically as affected by the baffle. At the smallest baffle distance ( $d/W = 5$ ), the confined slot-impinging jet with a baffle can fill in the local Nusselt number valley; however, as the Reynolds number increases, the accompanying second valley becomes more pronounced. Generally, both the valley and the second peak of the local Nusselt number gradually move downstream of the channel as the baffle distance increases. Moreover, the maximum second peak of the local Nusselt number at Reynolds numbers 100, 200, 300, and 400 occurs at $d/W = 5$, 10, 15, and 15, respectively. That is, the behavior of local heat transfer enhancement can be further controlled by adjusting the baffle distance at different flow velocities.

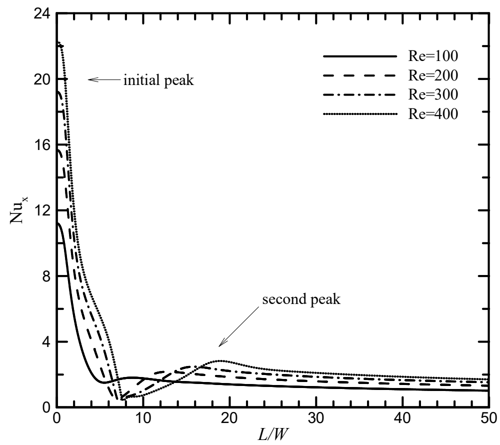


Fig. 6. Local Nusselt number profiles as a function of $L/W$ for different Re (normal case).

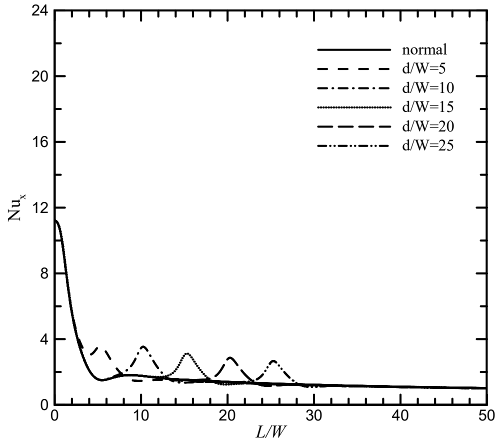


Fig. 7. Local Nusselt number profiles as a function of $L/W$ for different $d/W$ ( $\mathrm{Re}=100$ ).

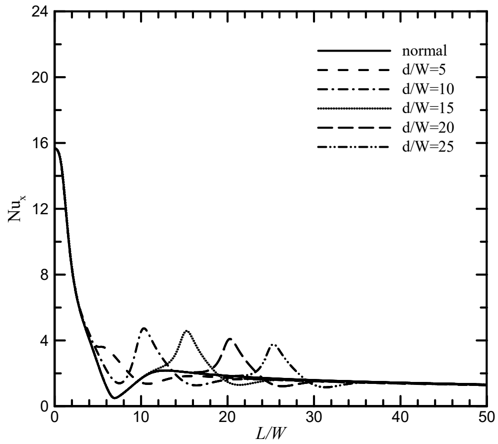


Fig. 8. Local Nusselt number profiles as a function of $L/W$ for different $d/W$ ( $\mathrm{Re}=200$ ).

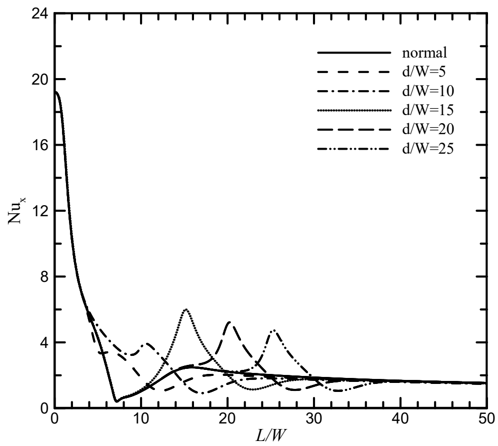


Fig. 9. Local Nusselt number profiles as a function of $L/W$ for different $d/W$ ( $\mathrm{Re}=300$ ).

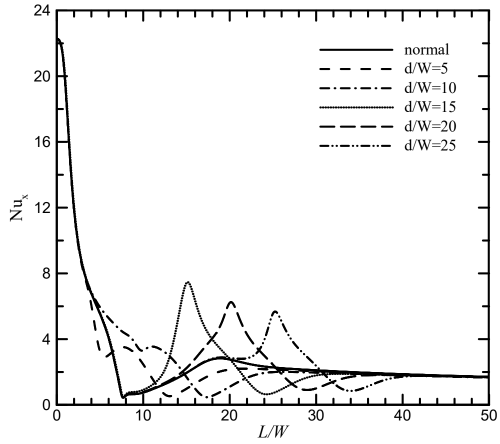


Fig. 10. Local Nusselt number profiles as a function of $L/W$ for different $d/W$ ( $\mathrm{Re}=400$ ).

Figures 11–14 illustrate the effect of baffle distance at Reynolds numbers in the range of 100−400 on the velocity distribution. First of all, in the normal case, it can be seen that the main stream of the fluid enters through the slot entrance, first impacts on the heated wall, then rebounds to the upper confined wall, then further rebounds downward, and finally exits along the downstream direction of the channel. From Figure 15, it can be observed that there are two distinct vortex structures around the main stream rebound transition of the fluid (adjacent to the confined wall and the heated wall). On the heated wall, the weaker vortex structure will lead to a decrease in heat transfer performance in the local area. In all the cases of adding a baffle, two types of baffle effect mechanisms can be found:

a. If the baffle is placed at the position where the fluid will rebound to the upper confined wall (include in front of this), the main stream of the fluid will be adjusted to flow against the heated wall by the action of the baffle, and the upward rebound of the main stream of the fluid will be weakened and delayed. Such a guided flow phenomenon can also be observed in Figure 16. This also results in more of the main stream of the fluid being able to exchange heat with the heated wall, further enhancing the heat transfer performance in the local area. In addition, two distinct vortex structures are generated at the front and rear of the baffle.

b. If the baffle is set farther away from the entrance of the slot, the main stream of the fluid is guided by the baffle to produce a phenomenon such as secondary impact, which further enhances the heat transfer performance in the local area. Overall, as the Reynolds number increases, the main stream rebound position of the fluid will gradually move towards the downstream direction of the channel, and the vortex structure will gradually expand.

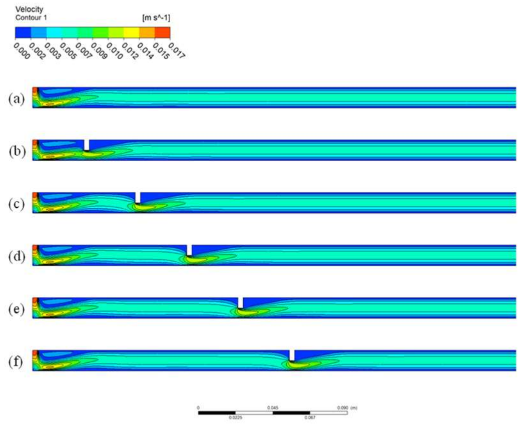


Fig. 11. Simulation contours of velocity, cases with $\mathrm{Re}=100$ : (a) normal case; (b) $d/W=5$ ; (c) $d/W=10$ ; (d) $d/W=15$ ; (e) $d/W=20$ ; (f) $d/W=25$ .

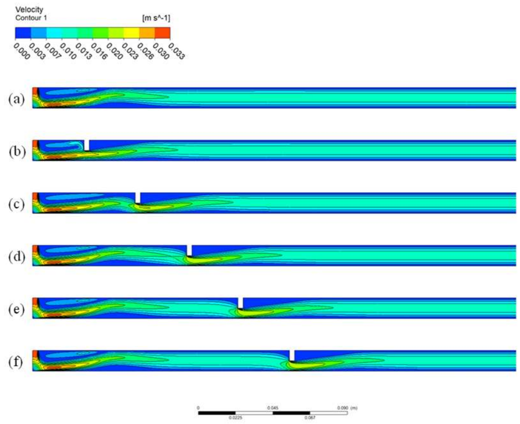


Fig. 12. Simulation contours of velocity, cases with $\mathrm{Re}=200$ : (a) normal case; (b) $d/W=5$ ; (c) $d/W=10$ ; (d) $d/W=15$ ; (e) $d/W=20$ ; (f) $d/W=25$ .

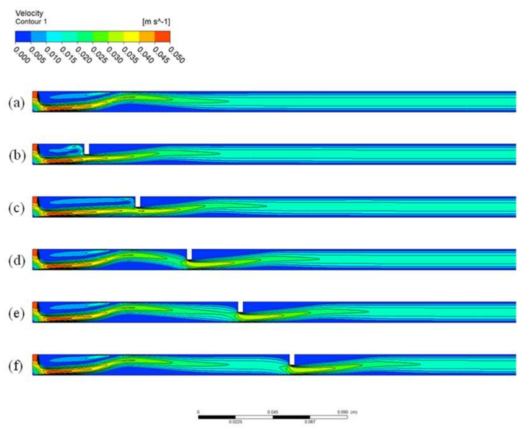


Fig. 13. Simulation contours of velocity, cases with $\mathrm{Re}=300$ : (a) normal case; (b) $d/W=5$ ; (c) $d/W=10$ ; (d) $d/W=15$ ; (e) $d/W=20$ ; (f) $d/W=25$ .

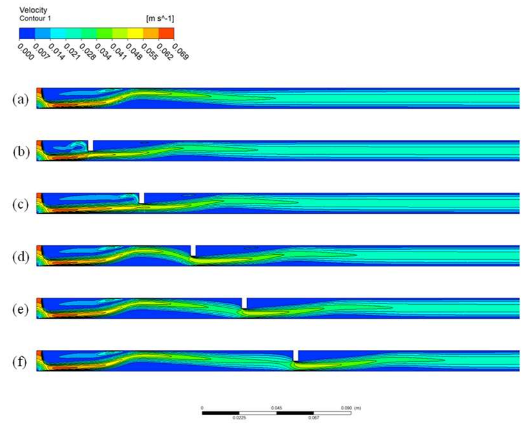


Fig. 14. Simulation contours of velocity, cases with $\mathrm{Re}=400$ : (a) normal case; (b) $d/W=5$ ; (c) $d/W=10$ ; (d) $d/W=15$ ; (e) $d/W=20$ ; (f) $d/W=25$ .

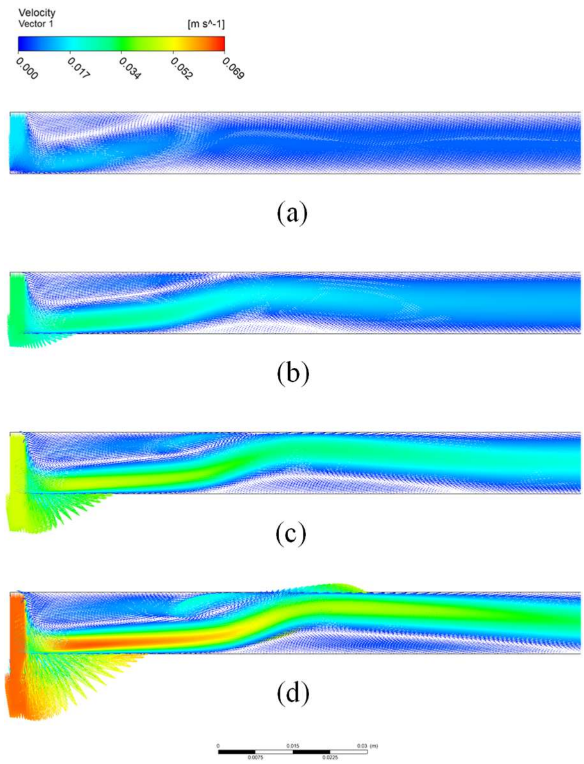


Fig. 15. Simulation contours of velocity vector, cases with normal case: (a) $\mathrm{Re}=100$ ; (b) $\mathrm{Re}=200$ ; (c) $\mathrm{Re}=300$ ; (d) $\mathrm{Re}=400$ .

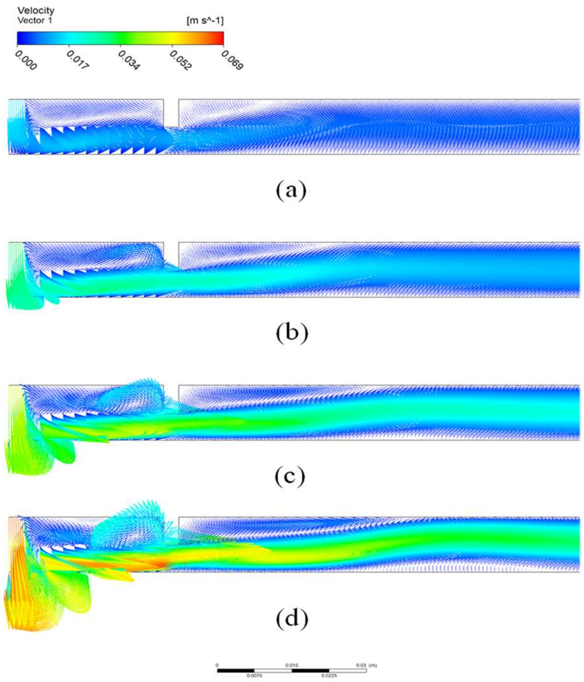


Fig. 16. Simulation contours of velocity vector, cases with $d/W = 5$ : (a) $\mathrm{Re} = 100$ ; (b) $\mathrm{Re} = 200$ ; (c) $\mathrm{Re} = 300$ ; (d) $\mathrm{Re} = 400$ .

Figures 17 and 18 depict the effects of the Reynolds number and baffle distance on the friction factor and the mean Nusselt number, respectively. In general, as the Reynolds number increased, the friction factor decreased. Compared to the normal case, when the baffle distance $d/W$ is greater than or equal to 15, the presence of the baffle results in a higher friction factor, indicating that the baffle increases the flow resistance within the channel. The velocity contour plots in Figs. 11(d)–(f) through 14(d)–(f) also reveal that the main stream, after rebounding from the upper confined wall, continues to develop downstream and is subsequently impeded by the baffle. However, in the cases with a baffle distance of $d/W \le 10$ , the friction factor gradually approaches that of the normal case as Re increases. In the case at $\mathrm{Re} = 400$ and $d/W = 5$ , the friction factor is even lower than that of the normal case. As shown in the velocity contour plots of Figs. 11(b)–(c) through 14(b)–(c), the flow-guiding effect of the baffle significantly reduces the velocity of the main stream rebounding toward the upper confined wall. As a result, the main flow transitions into a cross-flow pattern earlier, leading to a reduction in flow resistance within the channel. Figure 18 shows that the average Nusselt number increases gradually as the Reynolds number increases. To present a more detailed view of the variations, Figure 19 further illustrates the effect of baffle distance on the average Nusselt number. The solid, dashed, dash-dot, and dotted lines represent the average Nusselt numbers of the normal case at Reynolds numbers of 100, 200, 300 and 400, respectively. Compared with the normal case, the confined slot-impinging jet with a baffle exhibits a higher heat transfer performance, except for one particular case ( $\mathrm{Re} = 400$ , $d/W = 5$ ). By examining the phenomena in Figs. 10 and 14(b) for this particular case, it can be observed from the velocity contour plots that although the baffle redirects the main stream to follow along the heated wall, it also reduces the flow velocity as the fluid enters or exits the baffle region. This velocity reduction leads to lower local Nusselt numbers before the baffle and at the rebound location, ultimately resulting in a lower average Nusselt number compared to the normal case. As the Reynolds number increases, the maximum average Nusselt number gradually occurs at the longer baffle distance. The highest average Nusselt number is generated at $\mathrm{Re} = 400$ , $d/W = 15$ . The highest percentage increases in average Nusselt number is 6.02% at $\mathrm{Re} = 200$ and $d/W = 10$ . To evaluate the effectiveness of the baffle in enhancing heat transfer in a confined slot-impinging water jet, a performance evaluation criterion ( PEC ) is employed to assess whether the benefits of heat transfer enhancement outweigh the increase in flow resistance. Figure 20 illustrates the effects of the Reynolds number and baffle distance on the performance evaluation criterion. In all cases with $d/W \ge 15$ , although the performance evaluation criterion remains less than 1, it shows a gradually increasing trend as the Reynolds number increases. This indicates that at higher inlet velocities, installing a more distant baffle may have the potential to enhance the thermal performance of the confined slot-impinging jet. In the case of $d/W = 5$ , the performance evaluation criterion exhibits a peak at $\mathrm{Re} = 300$ , while in the case of $d/W = 10$ , the performance evaluation criterion gradually increases with increasing Reynolds number. Within the investigated range of baffle distances, the optimal performance evaluation criterion ( $\mathrm{PEC} = 1.0127$ ) occurs at $d/W = 10$ and $\mathrm{Re} = 400$ .

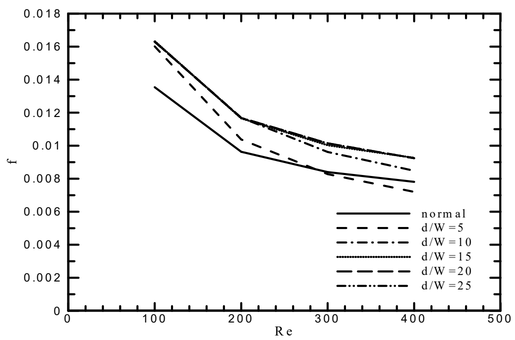


Fig. 17. Friction factor as a function of Re for different $d/W$ .

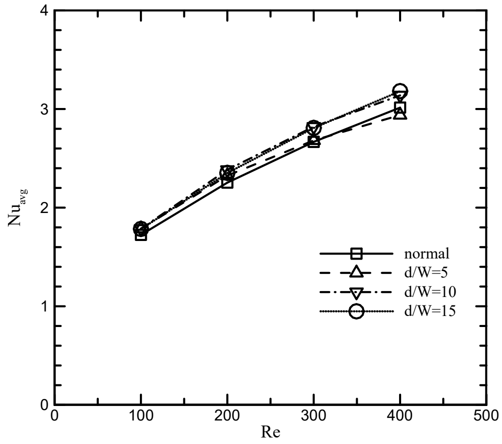


Fig. 18. Average Nusselt number as a function of Re for different $d/W$.

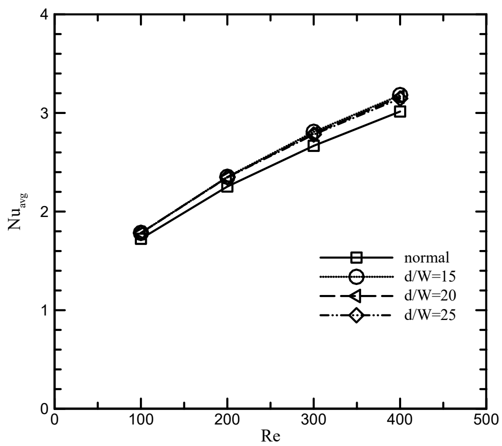


Fig. 18. *cont.*

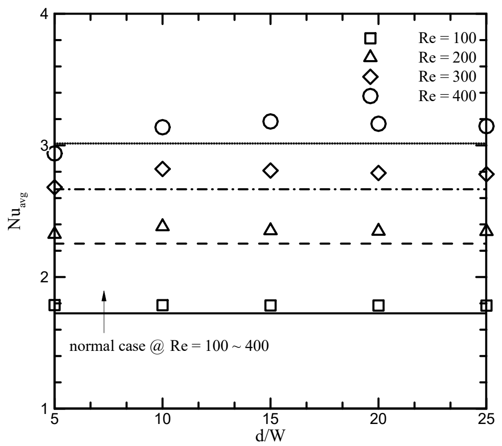


Fig. 19. Average Nusselt number as a function of $d/W$ for different Re.

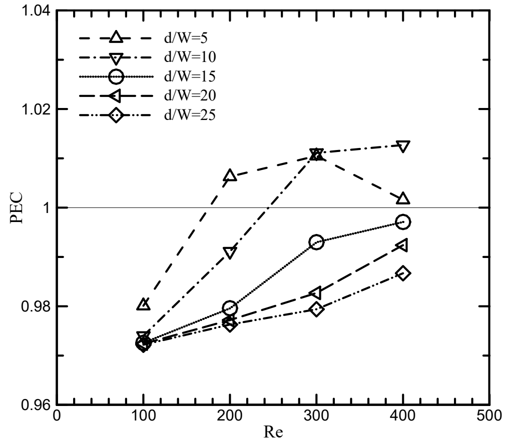


Fig. 20. Performance evaluation criterion as a function of Re for different $d/W$.

To further investigate whether the geometry of the baffle affects the thermal performance of the confined slot-impinging jet, this study extends the analysis to examine the effects of baffle height and width under the case with the optimal performance evaluation criterion ($d/W = 10$, $\mathrm{Re} = 400$). Figures 21 and 22 reveal the effects of the baffle height and width on the friction factor and the average Nusselt number, respectively. The results show that both the friction factor and the average Nusselt number increase gradually with the baffle height and width, with a particularly significant enhancement observed at a baffle height of $h_b/W = 1.5$. Figures 23–24 illustrate the effects of baffle height and width on the velocity distribution at a Reynolds number of 400. It can be observed that at the lowest baffle height ($h_b/W = 0.5$), the baffle is unable to effectively guide the main stream. As the baffle height increases, the baffle gradually begins to direct the main stream along the heated wall surface. Although at the highest baffle height ($h_b/W = 1.5$) the main stream accelerates upon exiting the baffle due to the contraction effect, the increased baffle height also results in greater flow resistance. On the other hand, as the baffle width increases, the baffle continuously guides the main stream along the heated wall, thereby enhancing the overall convective heat transfer. However, the reduced flow passage also leads to increased flow resistance within the channel. Figures 25 & 26 show the performance evaluation criteria for the confined slot-impinging water jet with a baffle, with the effects of baffle height and width investigated separately. It can be clearly observed from the figures that, due to the interaction between heat transfer enhancement and increased flow resistance, the optimal baffle height occurs at $h_b/W = 1.0$. Moreover, as the baffle width increases, the performance evaluation criterion can be further improved. In this study, the highest performance evaluation criterion ( $\mathrm{PEC}=1.0225$ ) value is obtained at $d/W=10$ , $h_b/W=1.0$ , $w_b/W=8$ , and $\mathrm{Re}=400$ .

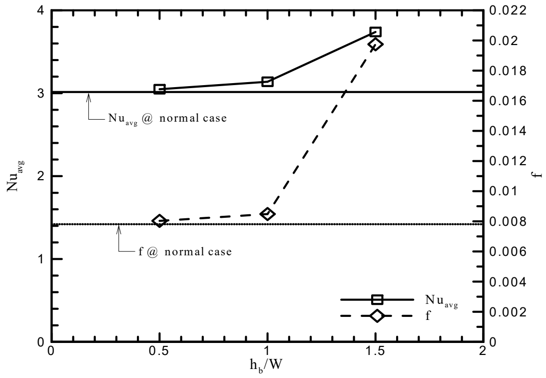


Fig. 21. Average Nusselt number and friction factor as a function of $h_b/W$ .

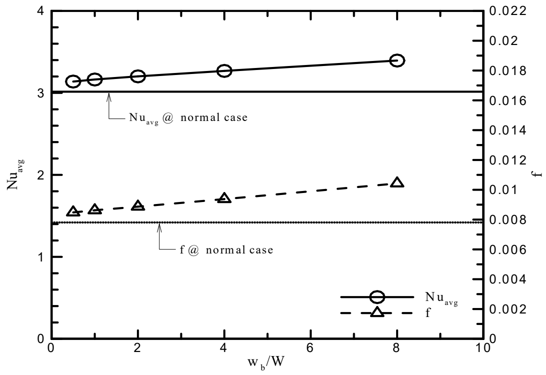


Fig. 22. Average Nusselt number and friction factor as a function of $w_b/W$ .

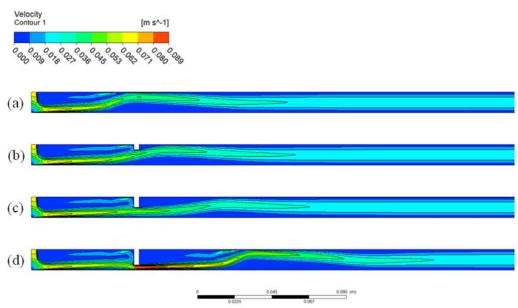


Fig. 23. Simulation contours of velocity, cases with $\mathrm{Re}=400$ : (a) normal case; (b) $h_b/W=0.5$ ; (c) $h_b/W=1.0$ ; (d) $h_b/W=1.5$ .

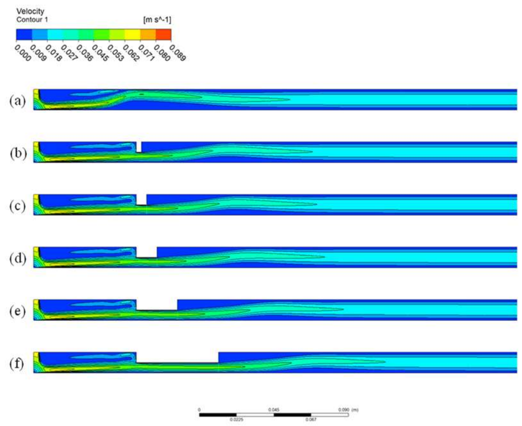


Fig. 24. Simulation contours of velocity, cases with $\mathrm{Re}=400$ : (a) normal case; (b) $w_b/W=0.5$ ; (c) $w_b/W=1.0$ ; (d) $w_b/W=2.0$ ; (e) $w_b/W=4.0$ ; (f) $w_b/W=8.0$ .

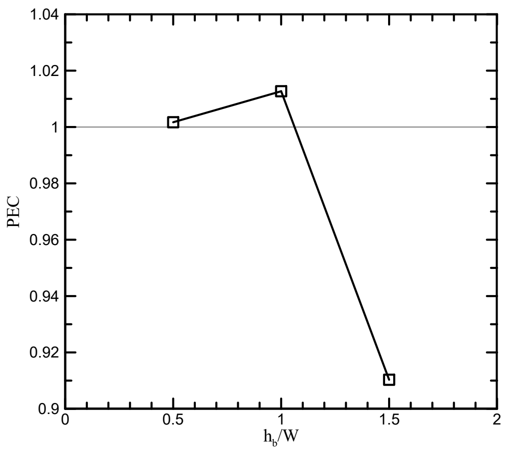


Fig. 25. Effect of baffle height on the variation of performance evaluation criteria at $\mathrm{Re}=400$ and $d/W=10$ .

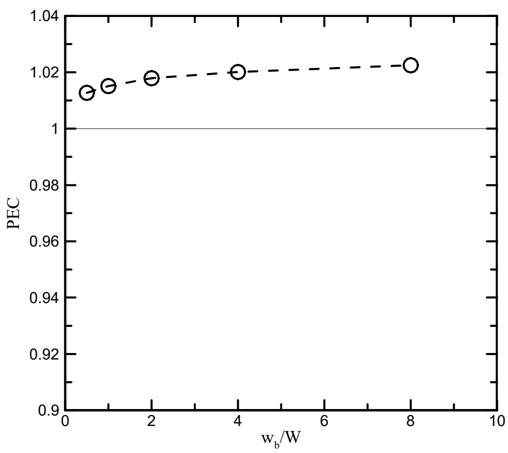


Fig. 26. Effect of baffle width on the variation of performance evaluation criteria at $\mathrm{Re}=400$ and $d/W=10$ .

## CONCLUSION

This study numerically investigated the fluid flow and heat transfer characteristics of a two-dimensional confined slot-impinging jet with a baffle through ANSYS-Fluent. Numerical simulations are conducted to analyze the effects of baffle distance ($5 \le d/W \le 25$), baffle height ($0.5 \le h_b/W \le 1.5$), and baffle width ($0.5 \le w_b/W \le 8.0$) on the thermal-flow fields and its corresponding characteristics for a range of Reynolds number ($100 \le \mathrm{Re} \le 400$). In addition, a uniform temperature is applied on the bottom wall. The numerical results of the pressure coefficient and stagnation point Nusselt number demonstrate a good agreement with the results of Lee et al. [4] and Chou and Hung [3]. This study shows that baffle placement has a strong impact on flow structure and heat transfer. The main stream flow pattern with the increase of the baffle distance produces two heat transfer mechanisms of guided flow and secondary impact respectively. When positioned near the main stream rebound point, the baffle redirects the flow toward the heated wall, enhancing local heat transfer. Downstream baffles induce secondary impingement, further improving performance. In all cases, two vortices form around the baffle, promoting mixing. As Reynolds number increases, the rebound point shifts downstream and vortices enlarge, suggesting that optimal baffle location depends on the Reynolds number. Overall, the analysis of thermal-flow characteristics reveals that as the Reynolds number increases, the average Nusselt number progressively increases, while the friction factor gradually decreases. The highest Nusselt number is observed at $\mathrm{Re} = 400$ and $d/W = 15$, while the largest relative enhancement (6.02%) occurs at $\mathrm{Re} = 200$ and $d/W = 10$. Moreover, baffles placed at larger distances ($d/W \ge 15$) increase flow resistance, resulting in a higher friction factor, whereas closer baffle placements ($d/W \le 10$) can reduce flow resistance at higher Reynolds numbers due to their flow-guiding effect. In terms of heat transfer, baffles consistently improve the average Nusselt number compared to the normal case, except at $\mathrm{Re} = 400$ and $d/W = 5$, where excessive flow deceleration before and after the baffle reduces thermal performance. Performance evaluation results suggest that while distant baffles ($d/W \ge 15$) increase resistance, their thermal performance improves at high Reynolds numbers. The optimal balance between heat transfer enhancement and flow resistance is achieved at $\mathrm{Re} = 400$ and $d/W = 10$, where the performance evaluation criterion reaches a maximum of 1.0127.

Furthermore, the results indicate that both baffle height and width significantly influence the thermal and flow characteristics of the confined slot-impinging jet. As either the baffle height or width increases, both the friction factor and average Nusselt number show a gradual rise, with notable thermal enhancement observed at a baffle height of $h_b/W = 1.5$. However, when the baffle is too short (e.g., $h_b/W = 0.5$), it fails to effectively guide the main stream, whereas increasing height improves flow guidance but also adds flow resistance. Similarly, increasing the baffle width enhances heat transfer by directing more flow along the heated wall, though this benefit comes at the cost of higher flow resistance due to reduced flow area. Based on the performance evaluation criterion, the optimal baffle geometry is achieved at $h_b/W = 1.0$, where the balance between heat transfer enhancement and flow resistance is most favorable. Furthermore, increasing baffle width up to $w_b/W = 8$ continues to improve the performance evaluation criterion. It can be concluded that the addition of baffle had a significant effect on the local heat transfer enhancement and an optimized value for the overall heat transfer enhancement. The highest thermal performance in this study is achieved at $d/W = 10$, $h_b/W = 1.0$, $w_b/W = 8$, and $\mathrm{Re} = 400$, with a maximum performance evaluation criterion of $\mathrm{PEC} = 1.0225$.

## REFERENCES

Chou, Y.J. and Hung, Y.H., "Impingement cooling of an isothermally heated surface with a confined slot jet," J. Heat Transfer., Vol. 116, No. 2, pp. 479–482(1994).

Gupta, A., Chougule, S.S., and Saha, S.K., "Cooling of highly concentrated photovoltaic cells with confined jet impingement by introducing channel configurations., Vol. 237, pp. 121600 (2024).

Herrada, M.A., Del Pino, C., and Ortega-Casanova, J., "Confined swirling jet impingement on a flat plate at moderate Reynolds numbers," Phys. Fluids, Vol. 21, pp. 013601(2009).

Hussain, L., Khan, M.M., Masud, M., Ahmed, F., Rehman, Z., Amanowicz, Ł., and Rajski, K., "Heat transfer augmentation through different jet impingement techniques: a state-of-the-art review," Energies, Vol. 14, No. 20, pp. 6458(2021).

Kumar S. and Vengadesan, S., "Control of separated fluid flow and heat transfer characteristics over a backward facing step," Numer. Heat Transf. A, Vol. 73, No. 6, pp. 366–384(2018).

Lee, H.G., Yoon, H.S., and Ha, M.Y., "A numerical investigation on the fluid flow and heat transfer in the confined impinging slot jet in the low Reynolds number region for different channel heights," Int. J. Heat Mass Transf., Vol. 51, No. 15–16, pp. 4055–4068(2008).

Lorenzo, G.D., Manca, O., Nardini, S., and Ricci, D., "Numerical study of laminar confined impinging slot jets with nanofluids," Adv.

Mech. Eng., Vol. 4, (2012).

Maghrabie, H.M., Attalla, M., and Abdelfattah, M., "Heat transfer intensification of a confined impinging air jet via a guiding baffle," J. Heat Mass Transfer., Vol. 145, No. 7, pp. 072301(2023).

Manca, O., Mesolella, P., Nardini, S., and Ricci, D., "Numerical study of a confined slot-impinging jet with nanofluids," Nanoscale Res. Lett., Vol. 6, pp. 188(2011).

Manca, O., Ricci, D., Nardini, S., and Lorenzo, G.D., "Thermal and fluid dynamic behaviors of confined laminar impinging slot jets with nanofluids," Int. Commun. Heat Mass Transf., Vol. 70, pp. 15−26(2016).

Mohammed, H.A., Alawi, O.A., and Wahid, M.A., "Mixed convective nanofluid flow in a channel having backward-facing step with a baffle," Powder Technol., Vol. 275, pp. 329–343(2015).

Molana, M. and Banooni, S., "Investigation of heat transfer processes involved liquid impingement jets: a review," Braz. J. Chem. Eng., Vol. 30, No. 3, pp. 413–435(2013).

Mookherjee, O., Pramanik, S., and Kar, U.K., "Numerical investigation of a confined laminar jet impingement cooling of heat sources using nanofluids," J. Heat Mass Transfer., Vol. 142, No. 8, pp. 082301(2020).

Nie, J.H., Chen, Y.T., and Hsieh, H.T., "Effects of a baffle on separated convection flow adjacent to backward facing step," Int. J. Therm. Sci., Vol. 48, No. 3, pp. 618–625(2009).

Oliveira, A.V.S., Maréchal, D., Lawrjaniec, D., and Gradeck, M., "Sweeping water jet ring quenching of a large steel bar near industrial conditions," Appl. Therm. Eng., Vol. 263, pp. 125305 (2025).

Pulat, E. and Beyazoglu, E., "Computational investigation of confined wall inclination effects on impinging jet fluid flow and heat transfer," Int. J. Therm. Sci., Vol. 163, pp. 106749(2021).

Qiu, S., Xu, P., Geng, L., Mujumdar, A.S., Jiang, Z., and Yang, J., "Enhanced heat transfer characteristics of conjugated air jet impingement on a finned heat sink," Therm. Sci., Vol. 21, No. 1A, pp. 279288(2017).

Selimefendigil, F., Oztop, H.F., and Chamkha, A.J., "Jet impingement heat transfer of confined single and double jets with non-newtonian power law nanofluid under the inclined magnetic field effects for a partly curved heated wall," Sustainability, Vol. 13, No. 9, pp. 5086(2021).

Seyedein, S.H., Hasan, M., and Mujumdar, A.S., "Turbulent flow and heat transfer from confined multiple impinging slot jets," Numer. Heat Transf. A, Vol. 27, No. 1, pp. 35–51(1995).

Singh, P., Aider, Y., and Kaur, I., "Swirl jet impingement heat transfer Effect of jet-to-target spacing, jet Reynolds number and orientation with flat target," Int. J. Therm. Sci., Vol. 184, pp. 107993(2023).

Weng, J-Y., Zhan, M-L., and Liu, Y-H.., "Experimental study of single and doublet liquid jet impingement on the liquid film of a horizontal heated plate," Heat Mass Transf., Vol. 61, pp. 44 (2025).

Xu, L., Yun, X., Xi, L., Gao, J., Yang, T., and Li, Y., "Heat transfer characteristics of single row of jets issuing from screw-thread nozzles impinging on a concave surface," Case Stud. Therm. Eng., Vol. 28, pp. 101590(2021).

Yalçinkaya, O., Özel, M.B., Durmaz, U., and Uysal, Ü., "Experimental heat transfer analysis of conical pin configurations in jet impingement cooling with elongated nozzle holes," J. Taiwan Inst. Chem. Eng., Vol. 164, pp. 105709 (2024).

Yousefi-Lafouraki, B., Ramiar, A., and Ranjbar, A.A., "Laminar forced convection of a confined slot-impinging jet in a converging channel," Int. J. Therm. Sci., Vol. 77, pp. 130–138(2014).